Multi-objective Optimization of Piezoelectric Actuator Placement for Shape Control of Plates using Genetic Algorithms

ARTICLE *in* JOURNAL OF MECHANICAL DESIGN · AUGUST 2009

Impact Factor: 1.25 · DOI: 10.1115/1.3160313

3 AUTHORS:

Rajesh Kudikala
The University of Sheffield
5 PUBLICATIONS **13** CITATIONS
SEE PROFILE

Kalyan Deb
Indian Institute of Technology Kanpur
244 PUBLICATIONS **24,176** CITATIONS
SEE PROFILE

Bishakh Bhattacharya
Indian Institute of Technology Kanpur
62 PUBLICATIONS **150** CITATIONS
SEE PROFILE

Multi-Objective Optimization of Piezoelectric Actuator Placement for Shape Control of Plates Using Genetic Algorithms

Rajesh Kudikala
Research Scholar
e-mail: kudikala@iitk.ac.in

Deb Kalyanmoy
Professor
e-mail: deb@iitk.ac.in

Bishakh Bhattacharya
Associate Professor
e-mail: bishakh@iitk.ac.in

Department of Mechanical Engineering,
IIT Kanpur,
Kanpur, 208016 India

Shape control of adaptive structures using piezoelectric actuators has found a wide range of applications in recent years. In this paper, the problem of finding optimal distribution of piezoelectric actuators and corresponding actuation voltages for static shape control of a plate is formulated as a multi-objective optimization problem. The two conflicting objectives considered are minimization of input control energy and minimization of mean square deviation between the desired and actuated shapes with constraints on the maximum number of actuators and maximum induced stresses. A shear lag model of the smart plate structure is created, and the optimization problem is solved using an evolutionary multi-objective optimization algorithm: nondominated sorting genetic algorithm-II. Pareto-optimal solutions are obtained for different case studies. Further, the obtained solutions are verified by comparing them with the single-objective optimization solutions. Attainment surface based performance evaluation of the proposed optimization algorithm has been carried out. [DOI: 10.1115/1.3160313]

1 Introduction

A recent technology that has been receiving much attention is that of the adaptive smart structures. These are structural systems whose shape and stiffness can be manipulated, while in operation, in order to change their electrical properties, mechanical behavior, or structural response. Among them, the shape control of adaptive structures using piezoelectric material has gained wide attention in the field of space structures. Shape control involves activating the structure in order to achieve a certain desired shape specified by the user. Crawley and de Luis [1] proposed the use of piezoelectric actuators as elements of intelligent structures. They modeled the bending and extensional actuation of cantilever beams by piezoelectric actuators and considered linear strain distribution for the piezoelectric material in transmitting strain to the substructure. Static and dynamic analytical models have been derived for segmented piezoelectric actuators that are either surface bonded to an elastic substructure or embedded in a laminated composite. Koconis et al. [2] addressed both direct and inverse problems of shape control. Though the problem of finding the voltage distribution to get the desired shape of the structure is addressed, the number of actuators required and their locations for obtaining the desired shape have not been addressed.

Mathew et al. [3] developed a finite element model of the piezoelectric actuated smart structure for active flow control applications and showed that the shear lag model gives better response prediction than the perfectly bonded model. The perfectly bonded model assumes that an infinitely rigid bond exists between the piezoelectric material and the substructure, with all loads from the piezoelectric material fully transmitted to the substructure. This creates an artificially stiff model. The shear lag model is used to improve the model by considering the effect of shear stress acting at the interface between the piezoelectric/bonding materials and the bonding material/substructure.

Chee et al. [4] developed a mixed model for composite beams with piezoelectric actuators and sensors. A third-order displacement theory has been used for finite element formulation. They developed a buildup voltage distribution (BVD) algorithm for the shape control of smart plate structures. They considered minimization of the squared difference between desired and actuated displacements as the objective function and obtained the distribution of voltage for achieving the desired shape. Sun and Tong [5] investigated the energy optimization for the local shape control of structures integrated with nonlinear piezoelectric actuators. They used the Lagrangian multiplier method to develop an algorithm to minimize the energy consumption with displacement constraints.

Optimization techniques such as genetic algorithms (GAs) and simulated annealing (SA) have also been used to determine the optimal actuator locations in truss structures for the correction of static deformations. Kincaid [6] applied the SA algorithm to the optimization of actuator placement in truss structures for static distortion minimization problem. Silva et al. [7] used single-objective binary coded GAs to solve the shape control problem and determined optimum voltages needed to apply to piezoactuators for achieving desired shape. Khorsand et al. [8] used genetic quantum algorithms (GQAs) to solve the optimization problem of shape control of the smart plate structures.

Majority of the studies reported posed the problem of shape control as a single-objective optimization problem. Optimizing multiple objectives like input energy, deviation/error, cost, etc., is computationally challenging and may be difficult to solve using classical optimization techniques. As most of these objectives are conflicting to each other, the multi-objective optimization problems will have a number of Pareto-optimal solutions rather than a single optimum solution. For finding all the Pareto-optimal solutions, we need to use population based evolutionary multi-objective (EMO) optimization algorithms.

In the current work the shape control of smart plate structures has been formulated as a multi-objective optimization problem to find out the optimal quantity and locations of the actuators and the required amount of voltages to be applied for getting the desired shape within a tolerable error limit along with the minimum input actuation energy. The objectives taken into consideration are minimization of input control energy and minimization of mean square

Manuscript received December 10, 2008; final manuscript received May 27, 2009; published online August 18, 2009. Review conducted by Nancy Johnson. Paper presented at the 2008 ASME Global Conference on Smart Materials, Adaptive Structures and Intelligent Systems (SMASIS2008), Washington, DC, October 28–30, 2008.

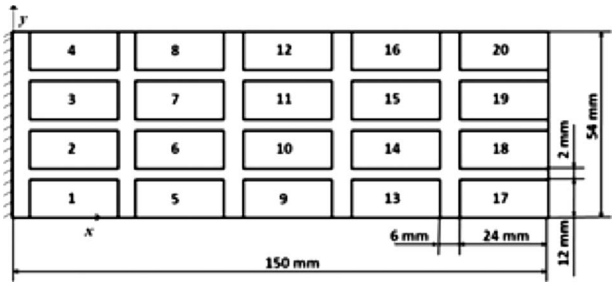

Fig. 1 Aluminum plate with 20 locations for the actuators

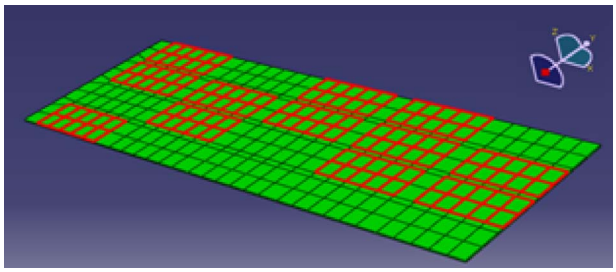

Fig. 2 Finite element model of the plate with actuators at the chosen locations

deviation between the desired and actuated shapes, subjected to constraints on the number of actuators and induced stresses. Shear lag models for the smart plate structures are created using ABAQUS [9], and the optimization problem is solved using an integrated approach with fast elitist nondominated sorting genetic algorithm (NSGA-II) [10]. The GA approach can handle multiple objectives simultaneously, without requiring the objectives to be combined to a single one [11]. With a view to increase confidence in the obtained Pareto-optimal solutions, they are verified by comparing with the single-objective optimization solutions.

Since convergence to the Pareto-optimal front and the maintenance of a diverse set of Pareto solutions are two distinct and somewhat conflicting goals of multi-objective optimization, no single metric can be used to decide the performance of an algorithm in an absolute sense. Fonseca and Fleming [12] suggested the concept of an attainment surface in the context of multi-objective optimization. Summary attainment surfaces (SAS) [13] obtained from multiple runs of an optimizer can be interpreted probabilistically for visualizing the performance of the optimization algorithm.

In Secs. 2 and 3, we describe the formulation of optimization problem followed by the integrated optimization approach for solving the problem and then we present the obtained Pareto-optimal solutions for few test cases of the rectangular and skew cantilever plates. Finally, the SASs obtained for all the cases for evaluating the performance of the proposed algorithm are discussed.

2 Optimization Problem Formulation

A cantilever aluminum plate of $150\times54\times0.5$ mm^3, with no applied mechanical load, is considered. The geometric model of the smart plate structure considered in the study is shown in Fig. 1.

On the top surface of the plate are shown the 20 locations considered for the placement of actuators (numbered from 1 to 20). The piezoelectric actuators are bonded to the top surface of the plate at the chosen locations with a finite thickness adhesive material. The thicknesses of actuators and bonding layer are 0.3 mm and 0.1 mm, respectively. The properties of the piezoelectric actuators are given in Table 1. The input voltage V_i applied to any actuator is limited to the range of -20V to 20V. The properties of the aluminum plate are Young's modulus $E_a=70$ GPa and Poisson's ratio $v_a=0.345$ and the properties of the bonding layer are Young's modulus $E_b=3$ GPa and shear modulus $G_b=1.07$ GPa. The finite element model of the aluminum plate and bonding layer is created using 20 node solid C3D20R elements, and the piezoelectric actuators are created using 20 node solid C3D20RE piezoelectric elements in ABAQUS [9]. The finite element model of the smart plate is shown in Fig. 2.

Table 1 Properties of P×5-N piezoelectric material [7]

C^E_{11} (N m^{-2})	13.11×10^{10}
C^E_{12} (N m^{-2})	7.984×10^{10}
C^E_{13} (N m^{-2})	8.439×10^{10}
C^E_{33} (N m^{-2})	12.31×10^{10}
C^E_{44} (N m^{-2})	2.564×10^{10}
C^E_{66} (N m^{-2})	2.564×10^{10}
d_{15} (mV^{-1})	515×10^{-12}
d_{31} (mV^{-1})	-215×10^{-12}
d_{33} (mV^{-1})	500×10^{-12}
$\varepsilon^{\sigma}_{11}/\varepsilon_0$	1800
$\varepsilon^{\sigma}_{33}/\varepsilon_0$	2100
ρ (kg m^{-3})	7800

Our algorithm evaluates various combinations of the number of actuators, locations, and applied voltages to find the optimal combination of these parameters. To model the presence or absence of an actuator in a location, the actual voltage range is doubled and new limits for x_i are chosen as 0–80 V. We have divided the range into three parts: 0–20 V, 20–60 V, and 60–80 V, which when transformed to original limits represent -20–0 V, 0 V, and 0–20 V, respectively, as illustrated in Fig. 3. In a NSGA-II population of solutions, a variable value falling in 0–20 V and 60–80 V ranges indicates the presence of an actuator, and the finite element analysis (FEA) model is created with the corresponding actuators in place and corresponding transformed voltages V_i applied. On the other hand a variable value falling in the range of 20–60 V indicates the absence of the actuator, and the FEA model is created without this actuator. A typical solution for five variables looks like $x_i=63.45$, 38.27, 62.52, 14.64, 22.90. It represents that the actuators in locations 1, 3, and 4 are present and the actuators in locations 2 and 5 are absent. The corresponding applied voltages V_1, V_3, and V_4 are 3.45 V, 2.52 V, and -5.36 V, respectively.

2.1 The Multi-Objective Optimization Problem. Minimize the input control energy (E) and the mean square deviation (F) between the desired and the actuated shapes subjected to constraints on induced stresses, number of actuators, and maximum acceptable deviation.

$$\text{Minimize } E=\sum_{i=1}^{n}[V_i^2/Z_i] \tag{1}$$

$$\text{Minimize } F=\frac{\sum_{j=1}^{N}[w_j^d-w_j^a]^2}{N} \tag{2}$$

$$\text{Subject to } \sigma_{\max\_in}\le\sigma_{\text{perm}} \quad \text{(for all materials)} \tag{3}$$

$$n\le10 \tag{4}$$

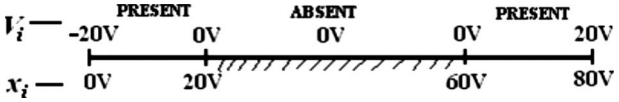

Fig. 3 Actuator presence/absence criteria

$$F \leq F^* \tag{5}$$

$$0 \leq x_i \leq 80, \quad i = 1,2,\ldots,20 \tag{6}$$

The above optimization problem involves 20 design variables, 2 conflicting nonlinear objective functions, and 3 inequality constraints. For solving the above multi-objective shape control problem, an integrated optimization approach is proposed, in which the NSGA-II is linked with the finite element analysis in ABAQUS. Few test cases of the rectangular plate and the skew plate have been considered for specifying the desired shapes. In this integrated approach for all population members, in each generation, the finite element model of the plate is created with the bonding layer and actuators in the chosen locations. Finite element analysis is done using ABAQUS to obtain nodal deflection values and induced stress values, which are plugged into the NSGA-II code for objective function evaluation.

The following parameter settings of NSGA-II are considered in the present study: Population size is 120, number of generations is 200, and probabilities of real parameter crossover and mutation are 0.9 and 0.05, respectively.

Various steps in the optimization algorithm are described below.

1. Set the NSGA-II parameters such as population size, number of generations, and crossover and mutation probabilities.
2. Initialize the population N.
3. For each population member, decide the presence/absence of the piezoelectric actuators from the values of the design variables. For the present actuators, voltage values are mapped to -20V to 20V. The finite element model of the plate is created with bonding layer and actuators in the chosen locations.
4. Finite element analysis is carried out in ABAQUS for each population member to obtain nodal deflection and induced stress values.
5. The obtained deflection and stress values are plugged back into NSGA-II.
6. Evaluate the objective function and constraints values.
7. Perform nondominated sorting of the population and assign front ranking.
8. Create offspring population using selection, crossover, and mutation operators.
9. Repeat Steps 3–5 and evaluate the objective function values for the offspring population.
10. Combine the parent and offspring population and assign front ranking based on nondominate sorting of combined population of $2N$.
11. Calculate the crowding distance and get the first N population members from the combined population.
12. Replace the old parent population with the new child population. Repeat the procedure in the next generation until the number of generations reaches the maximum number of generations.

In Sec. 3, we present four test cases considered for our study and the obtained optimal solutions.

3 Results

3.1 Case 1: Rectangular Plate. In case 1, for the rectangular plate shown in Fig. 1, the desired shape is described using a polynomial function as given by Eq. (7), which when evaluated gives the desired deflections specified to the set of points or nodes on the plate. These nodal deflections serve as input to the NSGA-II module.

$$W(x,y) = -(1.91x^2 + 0.88xy + 0.19x) \times 10^{-4} \tag{7}$$

The initial and desired shapes of the plate are shown in Fig. 4. Observe that by the nature of the polynomial function chosen to describe the desired shape, the plate is expected to experience

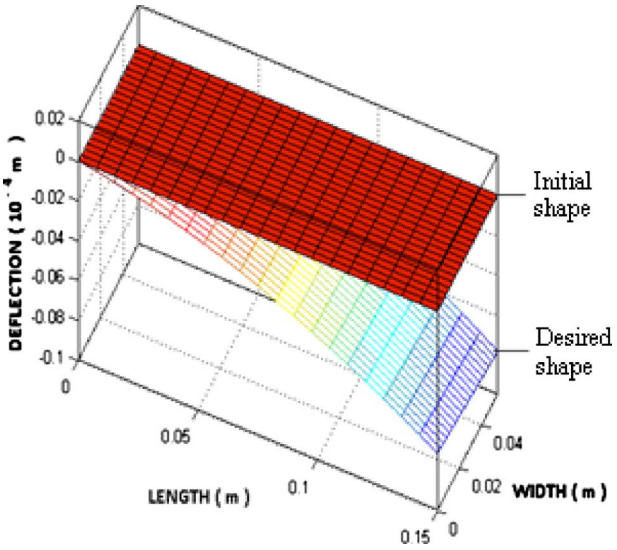

Fig. 4 Initial and desired shapes of the plate (case 1)

combined bending and twisting deformation. The multi-objective optimization problem as stated in Sec. 2 is solved using the proposed integrated optimization algorithm. The total computation time for solving the multi-objective optimization problem on a computer with an Intel Pentium 4 processor is estimated around 30 h.

Shown in Fig. 5 are the obtained Pareto-optimal (PO) solutions for the case of the desired shape illustrated in Fig. 4. It is observed that there are three different classes of solutions AB, BC, and CD with respect to the number and location of the actuators, as shown in Fig. 5. In the first class of solutions represented by region AB in Fig. 5, only five piezoelectric actuators in locations 1, 3, 6, 10, and 14 are active, whereas in the second class represented by BC, only seven actuators in locations 1, 3, 10, 14, 17, 18, and 20 are active, and in the third class represented by CD, only eight actuators in locations 1, 3, 11, 13, 17, 18, 19, and 20 are active. Figure 5 shows the locations of the active actuators in these three classes. This implies that as we move from A to D, the number of active

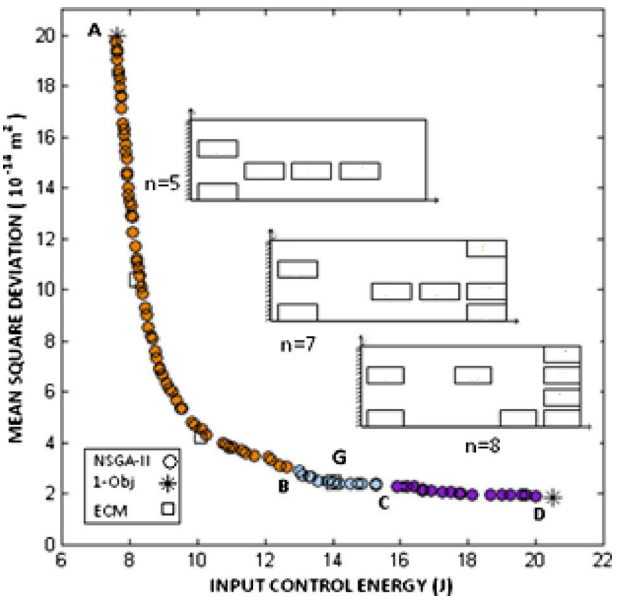

Fig. 5 Pareto-optimal solutions with optimal locations of the actuators (case 1)

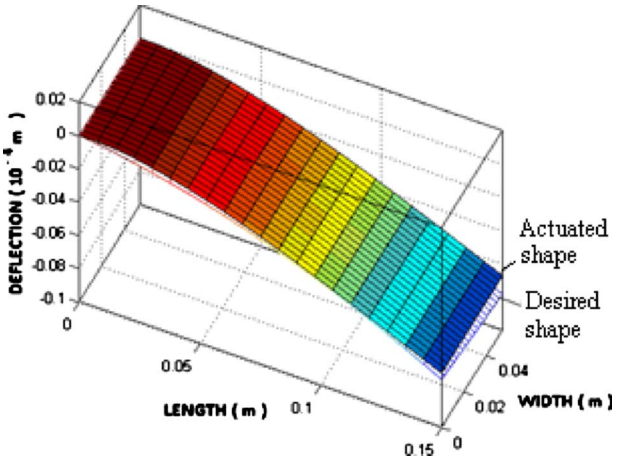

Fig. 6 Actuated and desired shapes at PO solution A

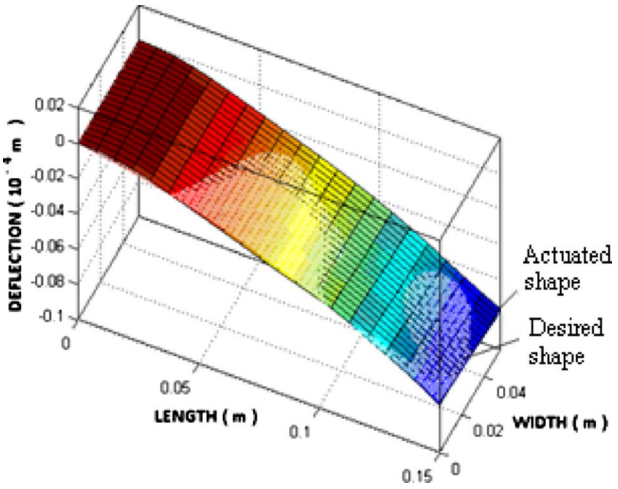

Fig. 8 Actuated and desired shapes at PO solution D

actuators and their locations are changing in order to decrease the mean square deviation between the desired and actuated shapes by consuming more actuation energy.

With a view to increase confidence in the Pareto-optimal solutions, a validation procedure has been performed. The two extreme PO solutions indicated by A and D correspond to the best solutions considering one of the two objectives E and F, respectively. Single-objective optimization has been performed using GA for each of the objectives E and F. The extreme PO solutions are validated with these single-objective (1-Obj) optimization solutions. Three intermediate solutions are validated with the solutions obtained from the epsilon-constraint method (ECM) [14] single-objective optimization, in which the objective function E is converted as a constraint: $E \leq 14$, 10, and 8. The individual 1-Obj and ECM single-objective solutions are shown in Fig. 5. The comparison of the actuated shapes with the desired shape at three PO solutions A, G, and D is shown in Figs. 6–8, respectively. The optimal voltage values applied to the present actuators at these solutions are listed in Table 2. It can be observed that as we move from solution A to D, the input actuation energy is increased, and the deviation between the desired shape and actuated shape is decreased. In this case, a minimum of 0.29% of the mean square deviation between the desired and initial shapes is achieved at PO solution D.

Crawley and de Luis [1] showed that for the maximum tip displacement in a bending configuration, the optimal location of the piezoelectric patch corresponds to the vicinity of the maximum strain, i.e., near the clamp location. In the present case also, the actuators in locations 1 and 3 are present in all PO solutions, which corresponds to the vicinity of the maximum strain. They contribute to a major portion of the required bending shape in comparison to the actuators near the free end to achieve the desired shape of the plate.

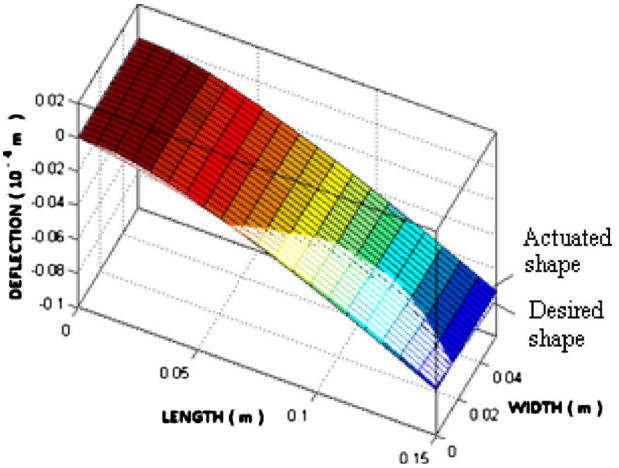

Fig. 7 Actuated and desired shapes at PO solution G

3.2 Case 2: Rectangular Plate. In case 2, the third mode shape of the cantilever rectangular plate is specified as the desired shape to the plate. Desired bending mode shape equation [15] is given by Eq. (8). Here, a is the length of the plate and b is the width of the plate.

$$W(x,y) = \sum_{m=1}^{p} \left\{ \left[A_{m1} + A_{m2}\sqrt{3}(1-2y/a) + \sum_{n=3}^{q} A_{mn} \left[\cosh\left(\frac{\varepsilon_n y}{b}\right) + \cos\left(\frac{\varepsilon_n y}{b}\right) - \alpha_n \left(\sinh\left(\frac{\varepsilon_n y}{b}\right) + \sin\left(\frac{\varepsilon_n y}{b}\right) \right) \right] \right] \left[\cosh\left(\frac{\varepsilon_m x}{a}\right) - \cos\left(\frac{\varepsilon_m x}{a}\right) - \alpha_m \left(\sinh\left(\frac{\varepsilon_m x}{a}\right) - \sin\left(\frac{\varepsilon_m x}{a}\right) \right) \right] \right\} \times 10^{-6} \quad (8)$$

Values of various parameters are taken from Ref. [15]. The initial and the desired shapes of the rectangular plate are shown in Fig. 9.

The PO solutions obtained for this case are shown in Fig. 10. It can be observed that there are three different classes of solutions AB, BC, and CD, with respect to the number and location of the piezoelectric actuators, as shown in Fig. 10. In the first class of

Table 2 Optimal voltage values at PO solutions A, G, and D

	PO solutions		
	A	G	D
E (J)	7.6082	14.0153	20.0133
F (10^{-14} m^2)	19.7698	2.4005	1.9163
Voltage applied to the present actuators V_i (V)	V_1=1.3334 V_3=2.0018 V_6=1.1306 V_{10}=0.6768 V_{14}=0.2944	V_1=1.4036 V_3=3.0185 V_{10}=1.0572 V_{14}=0.8276 V_{17}=0.8951 V_{18}=−0.1751 V_{20}=−0.5472	V_1=1.7693 V_3=3.0383 V_{11}=0.3426 V_{13}=1.9673 V_{17}=1.6753 V_{18}=−0.1193 V_{19}=−0.2805 V_{20}=−0.8745

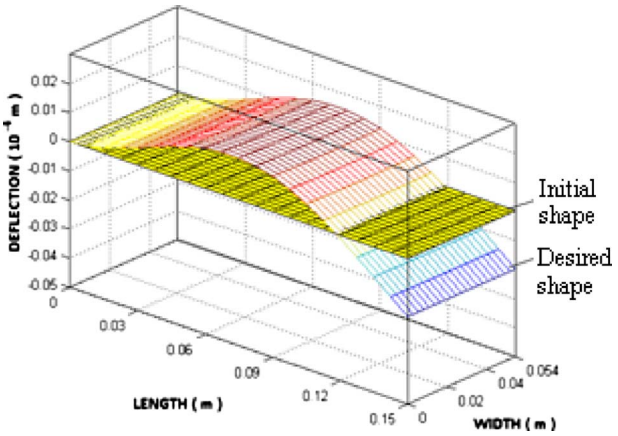

Fig. 9 Initial and desired shapes of the plate (case 2)

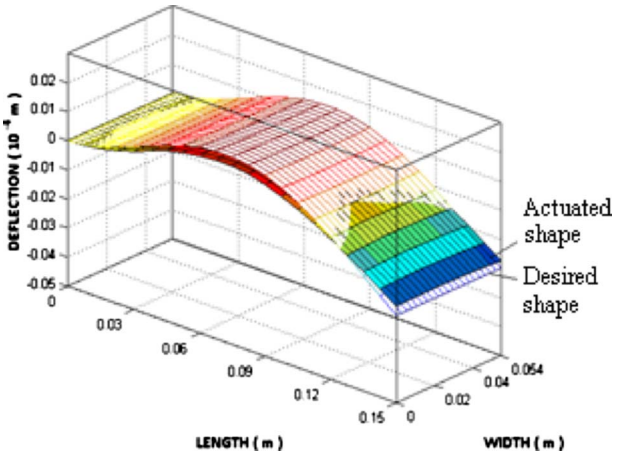

Fig. 11 Actuated and desired shapes at PO solution A

solutions represented by region AB in Fig. 10, only eight piezoelectric actuators in locations 2, 5, 8, 10, 12, 14, 16, and 19 are active, whereas in the second class represented by BC, only nine actuators in locations 2, 5, 8, 10, 12, 14, 16, 18, and 19 are active, and in the third class represented by CD, only nine actuators in locations 2, 4, 6, 8, 10, 12, 13, 15, and 19 are active. Figure 10 shows the number of active actuators and their locations in these three classes.

This implies that as we move from A to D, the number of active actuators and their locations are changing in order to decrease the mean square deviation between the desired and actuated shapes by consuming more actuation energy.

The obtained Pareto-optimal solutions are validated using single-objective optimization solutions. The extreme PO solutions are validated with individual single-objective solutions, and three intermediate solutions are validated with the ECM single-objective solutions. Figure 10 shows the individual single-objective and epsilon-constraint single-objective solutions. The comparison of the actuated shapes with the desired shape at three PO solutions A, G, and D is shown in Figs. 11–13, respectively. The optimal voltage values applied to the present actuators at these solutions are listed in Table 3. It can be observed that as we move from solution A to D, the input actuation energy is increased, and the deviation between the desired and actuated shapes is decreased. In this case, a minimum of 0.32% of the mean square deviation between the desired and initial shapes is achieved at PO solution D.

3.3 Case 3: Skew Plate. In this case, a skew cantilever aluminum plate with length $a=100$ mm, width $b=100$ mm, and skew angle $\alpha=15$ deg is considered, with 14 possible locations for the placement of the actuators. Figure 14 shows the geometric model of the skew plate. The skew plate is a limiting case of helicoidal shell shape. Shape control of the skew plates is useful

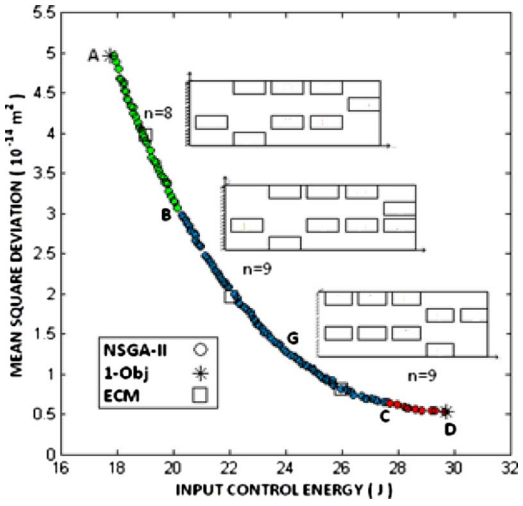

Fig. 10 Pareto-optimal solutions with optimal locations of the actuators (case 2)

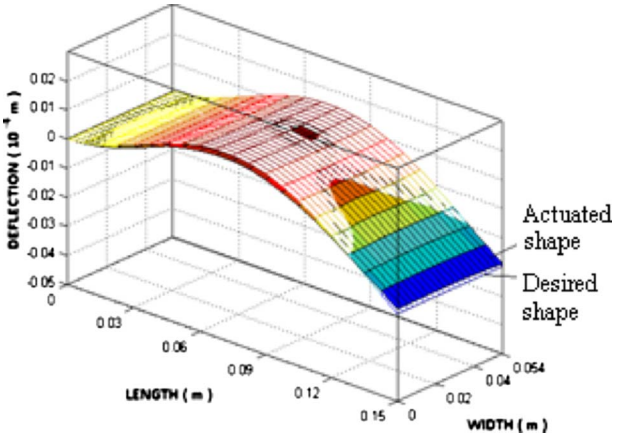

Fig. 12 Actuated and desired shapes at PO solution G

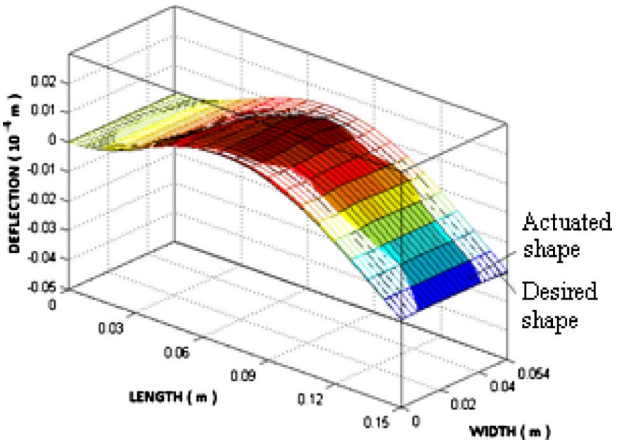

Fig. 13 Actuated and desired shapes at PO solution D

Table 3 Optimal voltage values at PO solutions A, G, and D

	PO solutions		
	A	G	D
E (J)	17.8951	23.1757	29.6914
F (10^{-14} m^2)	4.9658	1.5575	0.5288
Voltage applied to present actuators V_i (V)	V_2=−2.2811	V_2=−2.5605	V_2=−2.8366
	V_5=0.9252	V_5=0.9366	V_4=−1.1777
	V_8=1.3323	V_8=1.4706	V_6=1.8983
	V_{10}=1.9989	V_{10}=2.3113	V_8=1.0844
	V_{12}=1.6652	V_{12}=2.1437	V_{10}=2.4418
	V_{14}=1.3394	V_{14}=1.355	V_{12}=2.2389
	V_{16}=1.2059	V_{16}=1.3255	V_{13}=1.3925
	V_{19}=0.2093	V_{18}=−0.0207	V_{15}=1.5835
		V_{19}=0.2209	V_{19}=0.239

in applications like controlling the shape of aerofoil structures. Piezoelectric actuators with a length of 20 mm and a width of 20 mm are bonded to the skew plate at the chosen locations. The material properties of the actuators are given in Table 1. The transformations of the x- and y-coordinates into the ξ- and η-coordinates are given in Eq. (9).

$$\xi = \frac{x}{\cos(\alpha)}, \quad \eta = y - x\tan(\alpha) \tag{9}$$

The desired shape is described using a polynomial function as given by Eq. (10). Figure 15 shows the initial and desired shapes of the plate.

$$W(\xi,\eta) = -(1.562\xi^2 - 0.849\xi\eta + 0.289\eta) \times 10^{-4} \tag{10}$$

The multi-objective optimization problem is formulated with only 14 design variables as stated in the formulation and solved using the proposed integrated optimization algorithm.

Figure 16 shows the Pareto-optimal front obtained and optimum locations of actuators in the different classes of solutions. In this case there are four different classes of solutions AB, BC, CD, and DG, with respect to the number and location of the piezoelectric actuators, as shown in Fig. 16. In the first class of solutions represented by region AB in Fig. 16, only five piezoelectric actua-

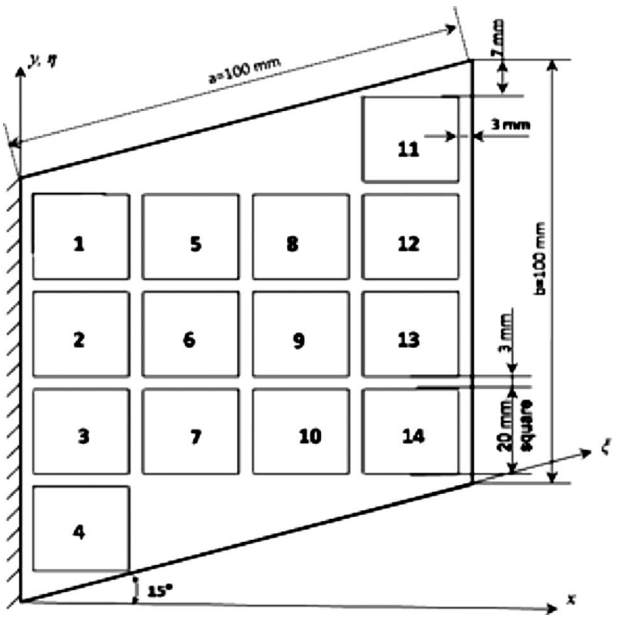

Fig. 14 Skew cantilever plate with 14 locations for the actuators

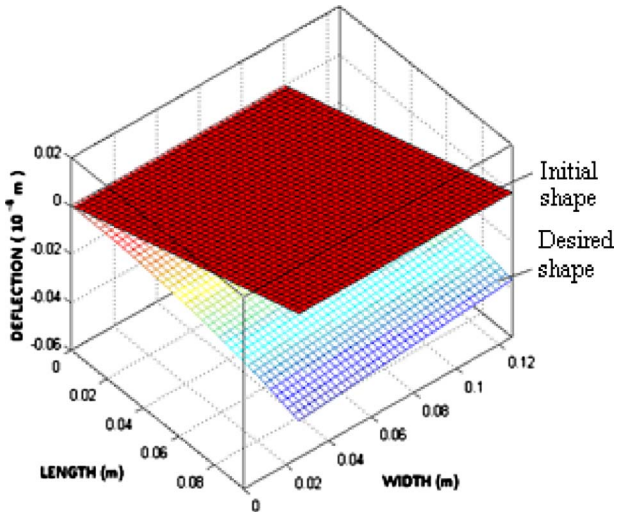

Fig. 15 Initial and desired shapes of the skew plate (case 3)

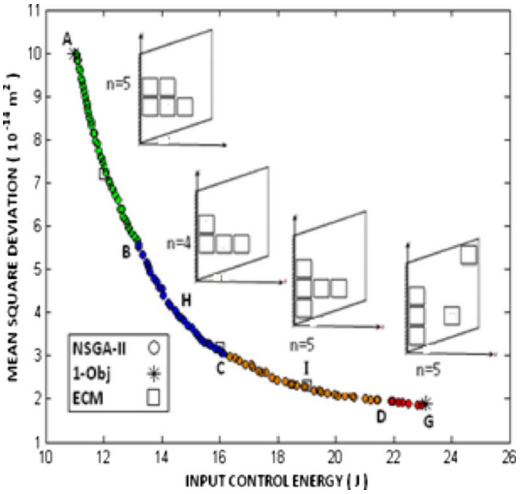

Fig. 16 Pareto-optimal solutions from NSGA-II with optimal locations of the actuators (case 3)

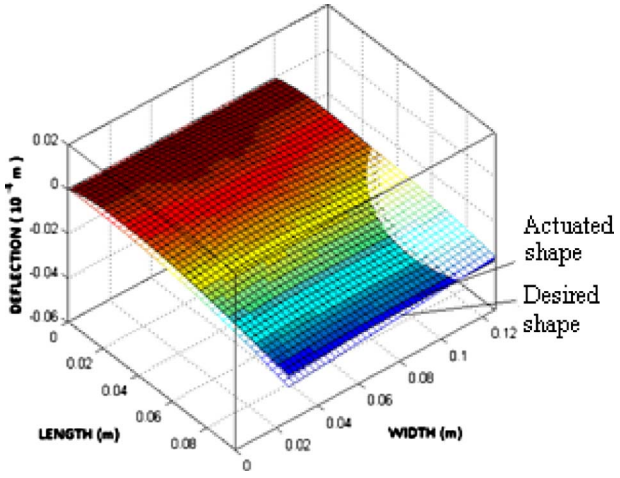

Fig. 17 Comparison of the desired and actuated shapes at PO solution A

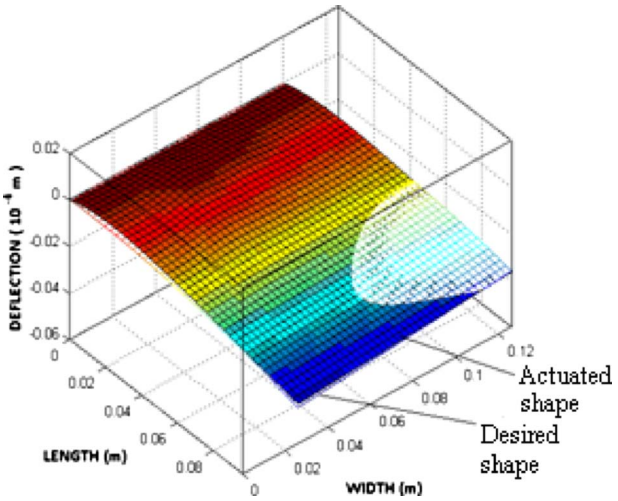

Fig. 18 Comparison of the desired and actuated shapes at PO solution H

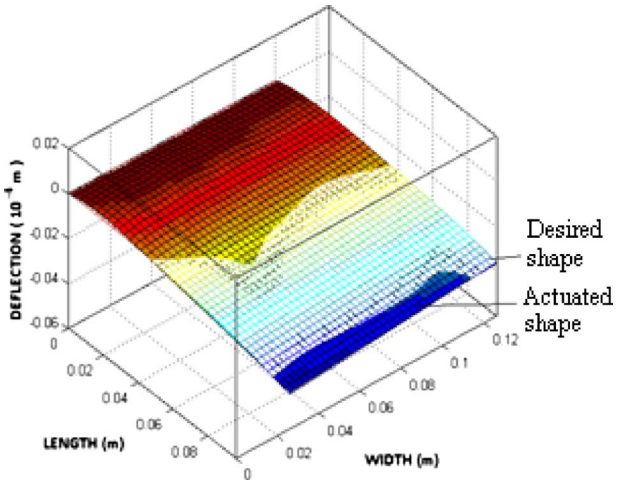

Fig. 20 Comparison of the desired and actuated shapes at PO solution G

tors in locations 2, 3, 6, 7, and 10 are active, whereas in the second class represented by BC, only four actuators in locations 2, 3, 7, and 10 are active, while in the third class represented by CD, only five actuators in locations 2, 3, 4, 7, and 10 are active, and in the fourth class represented by DG, only five actuators in locations 2, 3, 4, 10, and 11 are active. Figure 16 shows the active actuators and their locations in these three classes. The obtained Pareto-optimal solutions are validated using single-objective optimization solutions. Figure 16 shows the individual single-objective and epsilon-constraint single-objective solutions. The comparison of the actuated shapes with the desired shape at four PO solutions A, H, I, and G is shown in Figs. 17–20, respectively. The corresponding optimal voltage values applied to the active actuators for these solutions are listed in Table 4. In this case, a minimum of 0.56% of the mean square deviation between the desired and initial shapes is achieved at PO solution G.

3.4 Case 4: Skew Plate. In this case, the second mode shape of a cantilever skew plate is considered as the desired shape. The twisting mode shape equation is given by Eq. (11) [15]. In this, a is the length of the plate and b is the width of the plate, as shown in Fig. 14. The amplitude coefficients for the second mode shape and the eigenfunction parameter values are taken from Ref. [15]. The initial and the desired shapes of the skew plate are shown in Fig. 21.

$$W(\xi,\eta) = \sum_{m=1}^{p} \sum_{n=1}^{q} \frac{1}{2} A_{mn} \phi_m(\xi) \psi_n(\eta) \times 10^{-6} \qquad (11)$$

where

Table 4 Optimal voltage values at PO solutions A, H, I, and G

	PO solutions			
	A	H	I	G
E (J)	11.0592	14.2294	18.9535	22.9848
F (10^{-14} m^2)	9.9902	4.2202	2.2283	1.8765
Voltage applied to present actuators V_i (V)	V_2=2.0246 V_3=2.1442 V_6=1.0472 V_7=1.0305 V_{10}=0.4522	V_2=2.1496 V_3=2.7582 V_7=1.3635 V_{10}=0.3768	V_2=2.0467 V_3=2.815 V_4=2.5627 V_7=0.5199 V_{10}=0.0505	V_2=2.0949 V_3=3.3398 V_4=2.6742 V_{10}=0.4421 V_{11}=0.3088

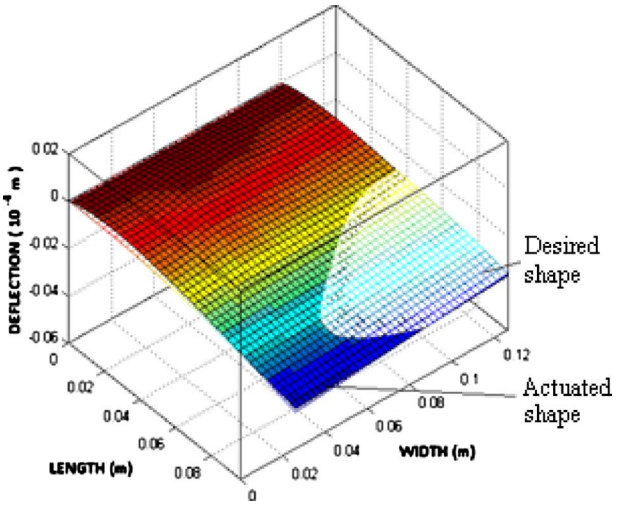

Fig. 19 Comparison of the desired and actuated shapes at PO solution I

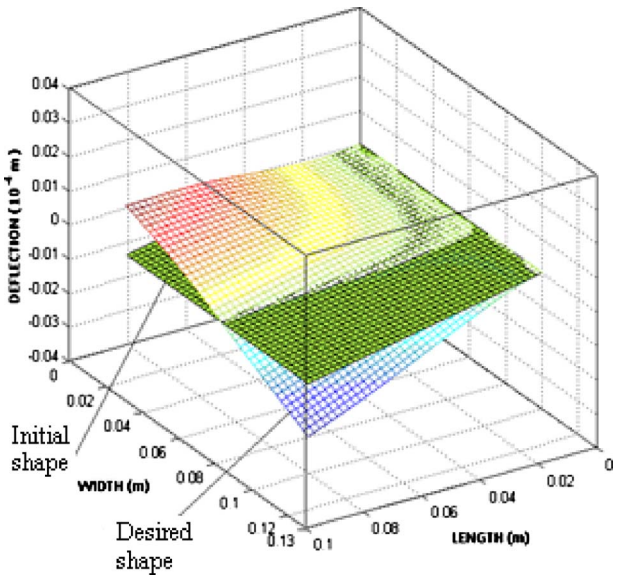

Fig. 21 Initial and desired shapes of the skew plate (case 4)

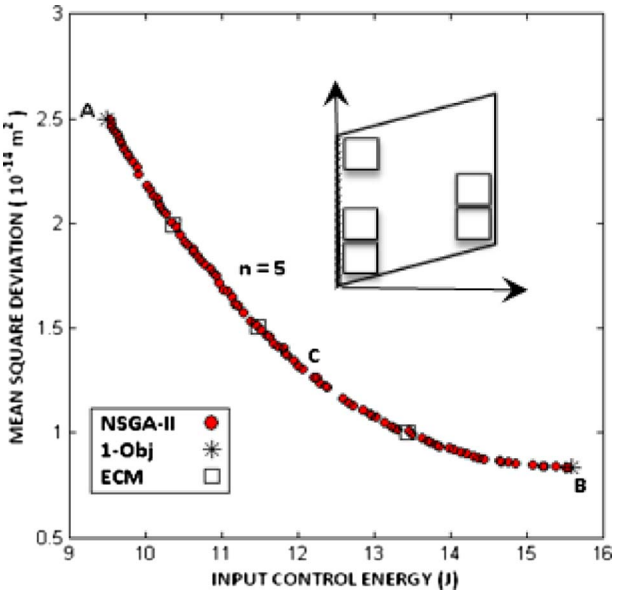

Fig. 22 Pareto-optimal solutions from NSGA-II with optimal locations of the actuators (case 4)

$$\phi_m = \cosh\left(\frac{\varepsilon_m \xi}{a}\right) - \cos\left(\frac{\varepsilon_m \xi}{a}\right) - \alpha_m\left(\sinh\left(\frac{\varepsilon_m \xi}{a}\right) - \sin\left(\frac{\varepsilon_m \xi}{a}\right)\right)$$

$$\psi_1 = 1$$

$$\psi_2 = \sqrt{3}(1 - 2\eta/b)$$

$$\psi_n = \cosh\left(\frac{\varepsilon_n \eta}{b}\right) + \cos\left(\frac{\varepsilon_n \eta}{b}\right) - \alpha_n\left(\sinh\left(\frac{\varepsilon_n \eta}{b}\right) + \sin\left(\frac{\varepsilon_n \eta}{b}\right)\right) \quad \text{for } n > 2$$

The optimization problem has been formulated with 14 variables. The desired deflections are calculated using Eq. (11) and specified to a set of nodes of skew plate. The PO solutions obtained for this case are shown in Fig. 22. Table 5 shows a representative set of Pareto-optimal solutions picked from the Pareto front shown in Fig. 22. The table gives the objective function and corresponding values of the voltage variables applied to the active actuators. It is observed that in this case, interestingly, the optimal number of actuators and their locations are same for all the Pareto-optimal solutions, unlike the different classes of solutions in the previous cases. In all the PO solutions, only five piezoelectric actuators in locations 1, 3, 4, 13, and 14 are active. Figure 22 shows the optimal locations of the piezoelectric actuators. The obtained Pareto-optimal solutions are also validated using single-objective optimization solutions. Figure 22 shows the individual

Table 5 Optimal voltage values at PO solutions A, C, and B

	PO solutions		
	A	C	B
E (J)	9.5204	12.2792	15.5562
F (10^{-14} m^2)	2.4961	1.2412	0.8364
Voltage applied to present actuators V_i (V)	V_1=1.7652	V_1=1.9581	V_1=2.2762
	V_3=−1.2573	V_3=−1.3632	V_3=−1.7637
	V_4=−1.8939	V_4=−2.1675	V_4=−2.2210
	V_{13}=0.4185	V_{13}=0.5485	V_{13}=0.3102
	V_{14}=1.0304	V_{14}=1.2601	V_{14}=1.4950

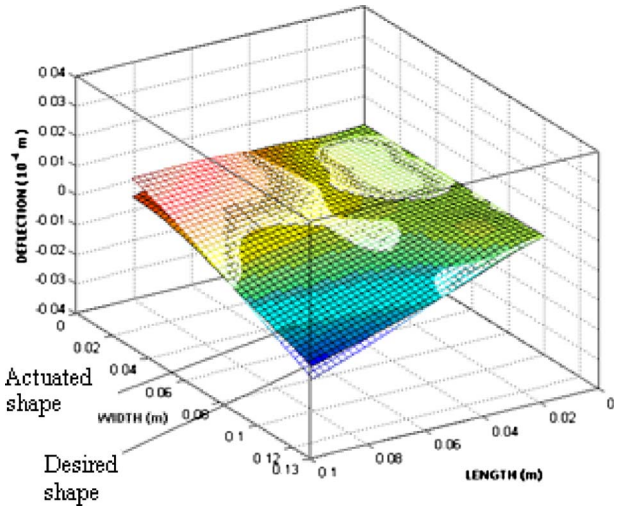

Fig. 23 Comparison of the desired and actuated shapes at PO solution A

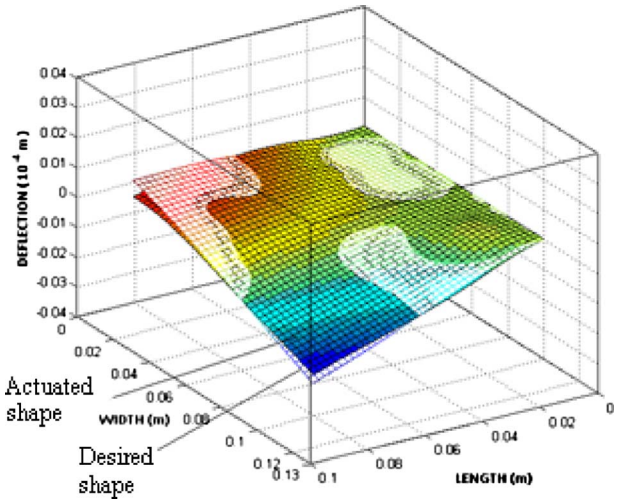

Fig. 24 Comparison of the desired and actuated shapes at PO solution C

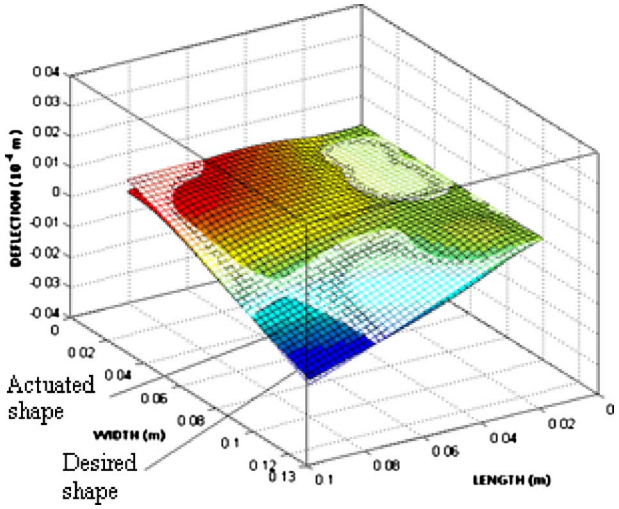

Fig. 25 Comparison of the desired and actuated shapes at PO solution B

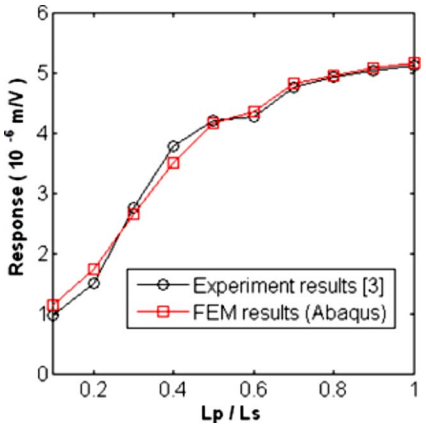

Fig. 26 Comparison of the responses from FEM and experiments [3]

1-Obj and ECM single-objective solutions. It can be seen that all the single-objective solutions are very close to Pareto front, which implies that the obtained Pareto-optimal solutions are diverse enough, and at the same time, very close to the global optimal solutions.

The comparison of the actuated shapes with the desired shape at three PO solutions A, C, and B is shown in Figs. 23–25, respectively. The corresponding optimal voltage values applied to the actuators for these solutions are listed in Table 5. It can be observed that moving from PO solution A to B, as the input actuation energy is increased, the deviation between the desired and actuated shapes is decreased. In this case, only a minimum of 0.99% of the mean square deviation between the desired and initial shapes is achieved at PO solution B.

To further validate the finite element analysis, a shear lag model of an aluminum plate surface bonded with piezoelectric actuator with finite thick adhesive layer (similar to Ref. [3]) has been simulated in ABAQUS. The comparison of the responses at the tip of the substructure, with increasing lengths of actuator L_P/L_S from 0.1 to 1 from the finite element model in ABAQUS and the experiments results [3], is shown in Fig. 26. The figure shows good agreement between the experimental and finite element model (FEM) responses. This shows the validity of the shear lag model created in ABAQUS.

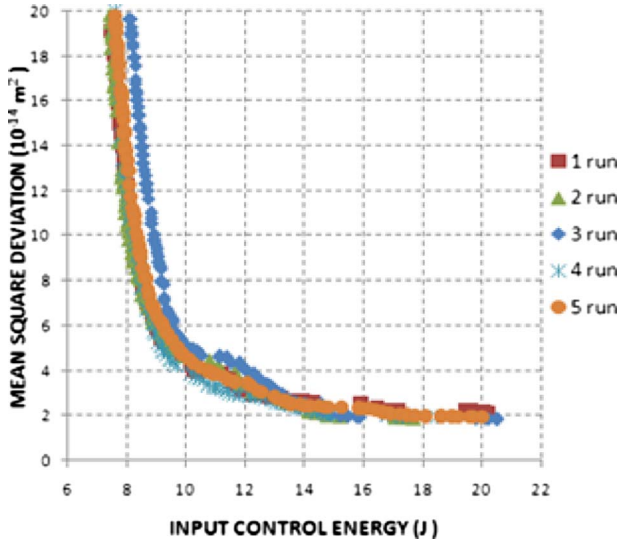

Fig. 27 Nondominated solutions in five runs (case 1)

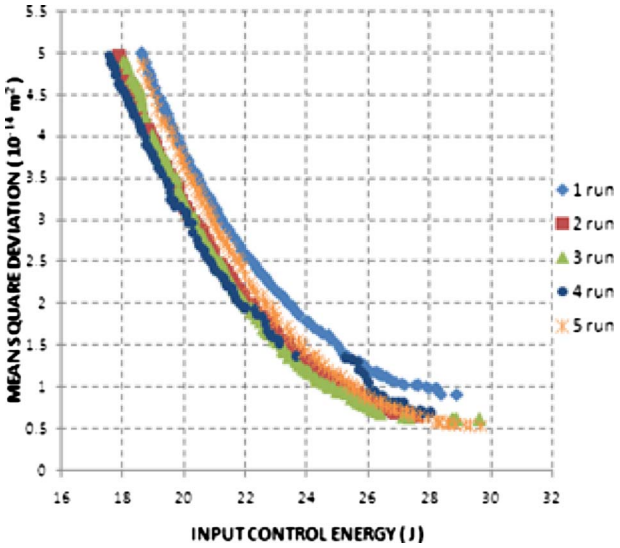

Fig. 28 Nondominated solutions in five runs (case 2)

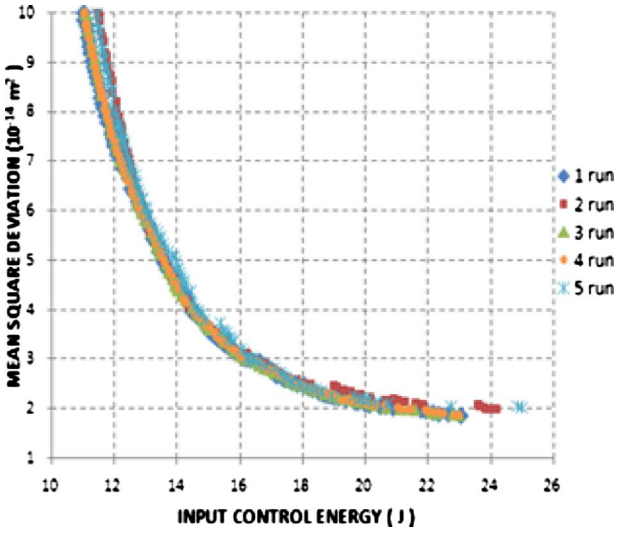

Fig. 29 Nondominated solutions in five runs (case 3)

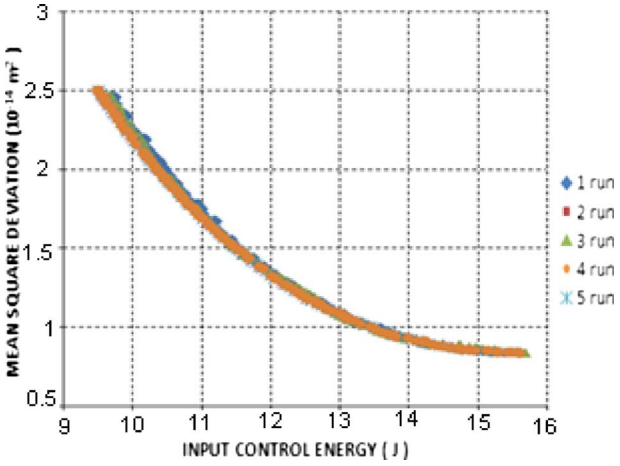

Fig. 30 Nondominated solutions in five runs (case 4)

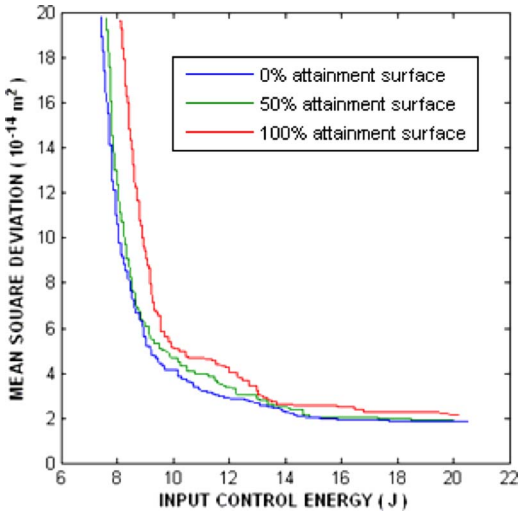

Fig. 31 The summary attainment surfaces (case 1)

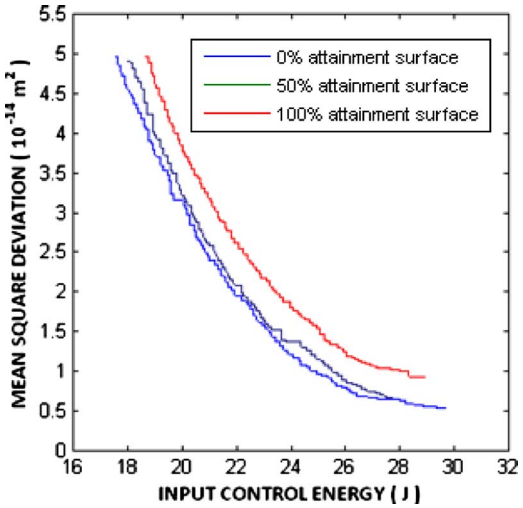

Fig. 32 The summary attainment surfaces (case 2)

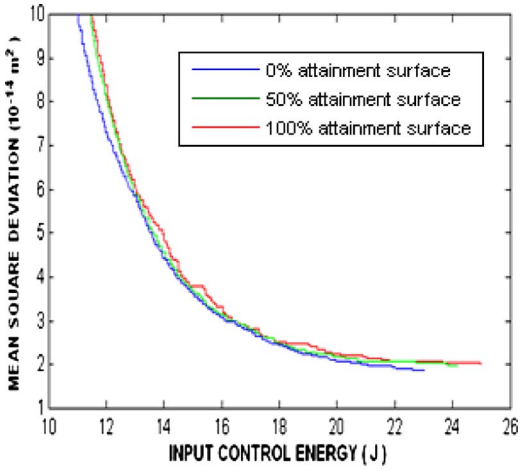

Fig. 33 The summary attainment surfaces (case 3)

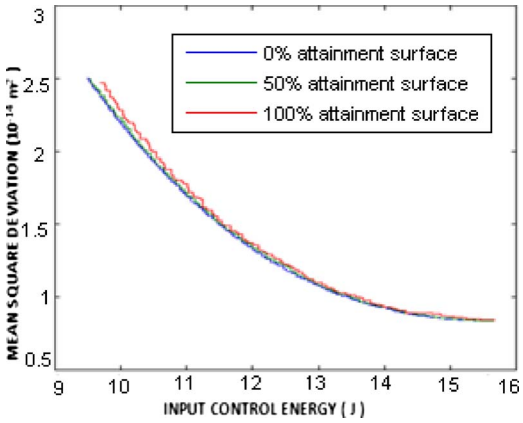

Fig. 34 The summary attainment surfaces (case 4)

3.5 SAS Based Performance Metric of Algorithm. When evaluating the performance of a stochastic optimization algorithm, it is sometimes desirable to express the performance in terms of the quality attained in a certain number of sample runs [12]. For evaluating the performance metric of the proposed algorithm for all the four cases, multiple runs with different initial populations are performed and summary attainment surfaces are obtained. Figure 27–30 show the nondominated solutions obtained in five runs of the algorithm with different initial populations in the four cases, respectively. The 0%, 50%, and 100% SASs obtained for all the four cases are shown in Figs. 31–34, respectively. The 50% SAS identifies the region of the objective space, which is dominated by half of the given SAS. Similarly the 0% SAS identifies the region not dominated by any of the given SAS, whereas 100% SAS identifies the region dominated by every given SAS. Thus, the 0% SAS visualizes the best case performance of the algorithm, while 100% SAS visualizes the worst-case performance of the algorithm.

The 0%, 50%, and 100% summary attainment surfaces in cases 1, 3, and 4 are very close to each other, whereas in case 2, the gap between 50% and 100% SAS is more. It is evident from the figures that the performance of the proposed algorithm is good in achieving the Pareto-optimal solutions very close to the actual Pareto front in all the cases.

4 Conclusions

In this work, the static shape control problem is formulated as a multi-objective optimization problem. An algorithm has been proposed in which based on a population member, the finite element model is created with actuators bonded at the chosen locations, and the calculated nodal deflection values are used for evaluating the values of the objective functions. By comparing with individual single-objective solutions and epsilon-constraint single-objective solutions, the obtained Pareto-optimal solutions are validated. The finite element model is also successfully validated with the experimental response values. The proposed integrated optimization approach is envisaged to be useful for solving the placement of actuators in more complex systems.

Acknowledgment

The authors would like to acknowledge the Indian Space Research Organization (ISRO) for partly sponsoring this work through Project No. ISRO-ME-2006-0030.

Nomenclature

A_{mn} = amplitude coefficients (m)
C^E = elastic coefficients at constant electric field (N m^{-2})
d = piezoelectric coefficient (mV^{-1})

E_a, E_b = Young's modulus of aluminum and bonding layer (N m^{-2})
E = input control energy (J)
F = mean square deviation between desired and actuated shapes (m^2)
F^* = 3% of mean square deviation between desired and initial shapes (m^2)
G = shear modulus (N m^{-2})
L_P = length of piezoelectric actuator (m)
L_S = length of substructure (m)
N = number of nodes with specified deflection
n = number of actuators present in the model
V_i = input voltage to the ith actuator (V)
w_j^a = actuated deflection at the jth node (m)
w_j^d = desired deflection at the jth node (m)
x_i = design variable in optimization (V)
x, y = coordinates of nodes (m)
Z_i = impedance of actuator (assumed to be 1.0 Ω)
α_m, α_n = eigenfunction parameters
ε^σ = dielectric coefficient (F m^{-1})
$\varepsilon_m, \varepsilon_n$ = eigenfunction parameters
ξ, η = mapped coordinates (m)
ρ = density (kg m^{-3})
$\sigma_{\max\_in}$ = maximum induced stress (MPa)
σ_{perm} = permissible stress of all materials (MPa)

References

[1] Crawley, E. F., and de Luis, J., 1987, "Use of Piezoelectric Actuators as Elements of Intelligent Structures," AIAA J., **25**(10), pp. 1373–1385.
[2] Koconis, D., Kollar, L., and George, S., 1994, "Shape Control of Composite Plates and Shells With Embedded Actuators II. Desired Shape Specified," J. Compos. Mater., **28**(3), pp. 262–285.
[3] Mathew, J., Sankar, B. V., and Cattafesta, L. N., 2001, "Finite Element Modeling of Piezoelectric Actuators for Active Flow Control Applications," AIAA Paper No. 2001-300.
[4] Chee, C., Tong, L., and Steven, G., 2000, "A Buildup Voltage Distribution (BVD) Algorithm for Shape Control of Smart Plate Structures," Comput. Mech., **26**(2), pp. 115–128.
[5] Sun, D., and Tong, L., 2005, "Energy Optimization in Local Shape Control of Structures With Nonlinear Piezoelectric Actuators," AIAA J., **43**(10), pp. 2210–2217.
[6] Kincaid, R. K., 1991, "Minimization Distortion in Truss Structures: A Comparison of Simulated Annealing and Tabu Search," 32nd AIAA/ASME/ASCE/AHS/ASC Structures, Structural Dynamics and Materials Conference, AIAA Paper No. 91-1095.
[7] Silva, S., Ribeiro, R., Rodrigues, J., Vaz, M., and Monteiro, J., 2004, "The Application of Genetic Algorithms for Shape Control With Piezoelectric Patches—An Experimental Comparison," Smart Mater. Struct., **13**, pp. 220–226.
[8] Khorsand, A. R., Akbarzadeh-T, M. R., and Moin, H., 2006, "Genetic Quantum Algorithm for Voltage and Pattern Design of Piezoelectric Actuator," IEEE Congress on Evolutionary Computation, pp. 2593–2600.
[9] ABAQUS/CAE FEA software, http://www.simulia.com/products/abaqus_fea.html.
[10] Deb, K., Agrawal, S., Pratap, A., and Meyarivan, T., 2002, "A Fast and Elitist Multi-Objective Genetic Algorithm: NSGA-II," IEEE Trans. Evol. Comput., **6**(2), pp. 182–197.
[11] Deb, K., and Kumar, A., 1995, "Real-Coded Genetic Algorithms With Simulated Binary Crossover: Studies on Multi-Modal and Multi-Objective Problems," Complex Syst., **9**(6), pp. 431–454.
[12] Fonseca, C. M., and Fleming, P. J., 1996, "On the Performance Assessment and Comparison of Stochastic Multi-Objective Optimizers," Proceedings of the Fourth International Conference on Parallel Problem Solving From Nature (PPSN)-IV, Vol. 1141, pp. 584–593.
[13] Knowles, J., 2005, "A Summary Attainment Surface Plotting Method for Visualizing the Performance of Stochastic Multi-Objective Optimizers," Proceedings of the Fifth International Conference on IEEE Intelligent Systems Design and Applications (ISDA-2005), pp. 552–557.
[14] Deb, K., 2001, *Multi-Objective Optimization Using Evolutionary Algorithms*, Wiley, Chichester, England.
[15] Leissa, A. W., 1969, "Vibration of Plates," NASA Paper No. SP-160.